

pubs.acs.org/macroletters Letter

Effect of Nanorod Physical Roughness on the Aggregation and Percolation of Nanorods in Polymer Nanocomposites

Shizhao Lu and Arthi Jayaraman*



Cite This: ACS Macro Lett. 2021, 10, 1416–1422



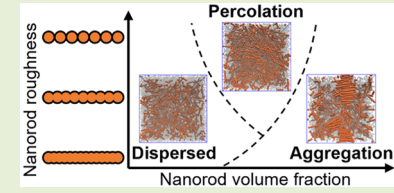
ACCESS

III Metrics & More

Article Recommendations

Supporting Information

ABSTRACT: Using molecular dynamics simulations, we elucidate the effect of nanorod roughness on nanorod aggregation, dispersion, and percolation in polymer nanocomposites (PNCs). By choosing coarse-grained models that enable systematic variation of the nanorod roughness and by selecting purely repulsive pairwise interactions for nanorods and polymer chains, we show how nanorod roughness affects the entropic driving forces for various PNC morphologies. At this entropically driven limit, we find that increasing nanorod roughness hinders nanorod aggregation and promotes nanorod percolation in the polymer melt. As



nanorod roughness increases, the nanorod volume fraction needed to induce nanorod aggregation also increases. Increasing nanorod roughness increases the configurational entropy of the polymer chains and lowers the entropically induced depletion attraction between nanorods.

Polymer nanocomposites (PNCs) with nanorods as fillers are useful in energy storage, 1-4 soft electronics, 5-8 and photonics^{9,10} applications, with the PNC functionality depending strongly on the nanorods' structure within the PNCs (i.e., dispersion, aggregation, orientational alignment, and percolation). The nanorod's structure in PNCs can be controlled by nanorod size (diameter and aspect ratio), chemistry, and surface functionalization. ^{11–13} A fluid of infinitely thin, hard spherocylinders transitions from a dispersed and unaligned (isotropic) phase to an aggregated and aligned (nematic) phase as the volume fraction of the spherocylinders increases, with the isotropic-nematic transition volume fraction predicted to be the inverse of the spherocylinder aspect ratio.¹⁴ When smooth nanorods are placed in a polymer melt, the entropically driven depletion—attraction interaction favors nanorod aggregation. Percolation ¹⁵ (i.e., an infinitely spanning network of particles) and factors affecting percolation, such as aspect ratio, ^{16,17} dispersity, ^{18–21} nanorod alignment, ^{15,22–24} and nanorod contact distance, ^{16,17,25} have been well studied in the context of smooth spherocylinders.

While the above fundamental studies are focused on smooth spherocylinders, practically found nanorods exhibit surface roughness that can affect their phase behavior. $^{26-28}$ For spherical nanoparticles, theory, $^{29-31}$ simulation, 32 and experiments 33 have shown that surface roughness can decrease the depletion—attraction between the spherical nanoparticles. This is due to free volume gain for the polymer/solvent of small diameter around the nanoparticles' rough crevices. 33 In a polymer solution, a spherical nanoparticle is considered rough when the R_g of the polymer is less than the size of the rough crevices; 32 in a polymer melt, the relevant roughness length scale is the diameter of a monomer. 34 In a polymer melt, at constant spherical nanoparticle roughness, as the monomer diameter decreases, nanoparticles aggregate, become dispersed,

and then aggregate again.²⁹ This nonmonotonic behavior of the rough nanoparticles' dispersion/aggregation with changing monomer diameter is attributed to a competition of the available free volume gain of the polymer at the rough ridges of the nanoparticle and the entropic penalty to enter those rough ridges. Even though many simulation studies have focused on the morphology^{13,35-40} and dynamics⁴¹⁻⁴⁴ of nanorods in a polymer melt using coarse-grained models of nanorods with overlapping beads or connected coarse-grained beads, to the best of our knowledge, studies have not demonstrated how varying *nanorod roughness* resulting from varying extents of overlap in nanorod model beads impacts the phase behavior of nanorods in the polymer melt, which is addressed in this letter.

We model the matrix polymer as a flexible bead–spring⁴⁵ chain of coarse-grained (CG) beads, each of diameter 1d representing a Kuhn segment of the polymer (Figure 1a) with equilibrium bond distance of 1d and a force constant of $50kT/d^2$. We model nanorods of length L as rigid bodies⁴⁶ (using the rigid/nvt/small fix command in the LAMMPS package⁴⁷) of CG spherical beads, each of diameter D. Nanorod roughness is varied by changing the extent of overlap of the CG beads (Figure 1b). The highest nanorod roughness (= 4) is achieved when there is no overlap between the CG beads, and the smoothest nanorod (= 0) has the most overlap of all cases studied in this letter; note that roughness 0 is not a smooth spherocylinder. In the Supporting Information (SI) Figures

Received: August 2, 2021 Accepted: October 18, 2021 Published: October 22, 2021





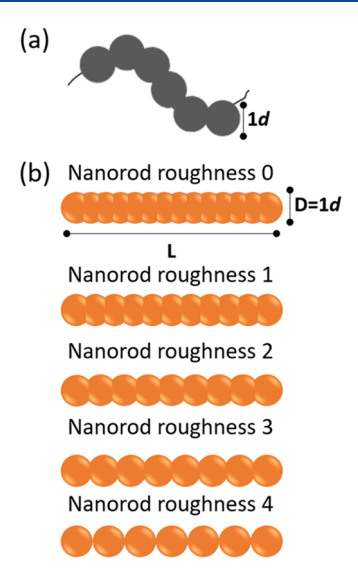


Figure 1. Coarse-grained model of the (a) matrix polymer chain and (b) nanorods of varying roughness. For all nanorods, the diameter is D (in units of d), and length is L (in units of d).

S1—S3 and Table S1, we present additional details about the nanorod model, in particular, the nanorod occupied and inaccessible volume for varying roughness values versus that of an ideal spherocylinder with identical dimensions; we also connect the model nanorod roughness to the roughness dimensions one would measure in realistic nanorods. The mass of the polymer CG beads and nanorod CG beads is fixed at 1 Lennard-Jones⁴⁸ mass units in the LAMMPS package.⁴⁷ This choice results in nanorod masses varying with nanorod roughness, with the mass of the smoothest nanorod being larger than the mass of the roughest nanorod; however, the choice of these nanorod masses does not affect the equilibrium structural properties of the PNCs, as we show in Figure S4.

The nonbonded interactions between all pairs of beads (i.e., nanorod CG bead and polymer CG bead) are modeled with the purely repulsive, Weeks—Chandler—Andersen⁴⁹ (WCA) potential where $\epsilon_{\text{WCA}} = 1kT$, $\sigma_{\text{WCA}} = (\sigma_i + \sigma_j)/2$, and σ_i and σ_j are the diameters of the i and j nonbonded CG beads. The nonbonded interactions between nonadjacent beads on the same nanorod are set to zero. Through the choice of these nonattractive interaction potentials, we expect the entropic driving forces to be dominant in dictating the equilibrium morphology of the PNC.

We run molecular dynamics (MD) simulations in the canonical ensemble at reduced temperature $T^* = 1$ using the LAMMPS⁴⁷ package. The temperature is maintained with the Nosé-Hoover thermostat.⁵⁰ We prepare the initial configuration by randomly placing (without any overlap) the nanorods and polymer chains in extended conformations in an initially large simulation box. We maintain periodic boundary conditions in all directions of the cubic simulation box. The matrix chains in unphysical (initial) extended configurations are relaxed and mixed with the nanorods over 30 million time steps with one time step equal to 0.0005τ , where τ is the reduced unit of time. Then, the large simulation box is gradually reduced in size over another 110 million time steps to achieve a final simulation box with a meltlike occupied volume fraction, $\eta = 0.35$. The above protocol ensures that the initial configuration used for the next stage (equilibration) has well-mixed chains and nanorods with the

chains in a relaxed configuration. We then equilibrate that meltlike PNC system for 180 million time steps. After the equilibration, we collect configurations every 1 million time steps during the production stage of 20 million time steps. We run three replicate simulation trials for each system. We calculate pair correlation functions, nanorod orientational order, nanorod cluster size, and percolation probability as described in the Supporting Information. We report the mean and standard deviation from the (20 configurations/trial \times 3 trials =) 60 configurations sampled.

We consider two matrix polymer chain lengths: N=20 and N=80; their (neat polymer) radius of gyrations ($R_{\rm g}$) simulated with the same bead—spring model as the PNCs in this study are $2.31\pm0.01d$ and $4.94\pm0.02d$, respectively. We consider nanorods of D=1d (Kuhn segment of the polymer) and L=7d. Thus, the nanorod length lies between the $2R_{\rm g}$ of the N=20 and N=80 polymers, and the nanorod diameter is commensurate with the Kuhn segment of the polymer. We consider PNCs with nanorod volume fraction ϕ varied from 0.10 to 0.20.

In the SI Table S2, we provide the number of nanorods (ranging from \sim 700–950), number of solvent beads/polymer chains (ranging from 60 000 to 300 chains depending on the matrix polymer chain length), and the simulation cubic box sizes (ranging from \sim 36d to \sim 46d) chosen to arrive at the desired nanorod volume fraction ϕ ranging from 0.10 to 0.20.

In PNCs with an N=80 polymer matrix, the roughest L=7d nanorods (roughness 4) remain dispersed at a nanorod volume fraction of $\phi=0.16$, while the two smoother nanorods (roughness 2 and 0) aggregate as seen in Figure 2a–c. The

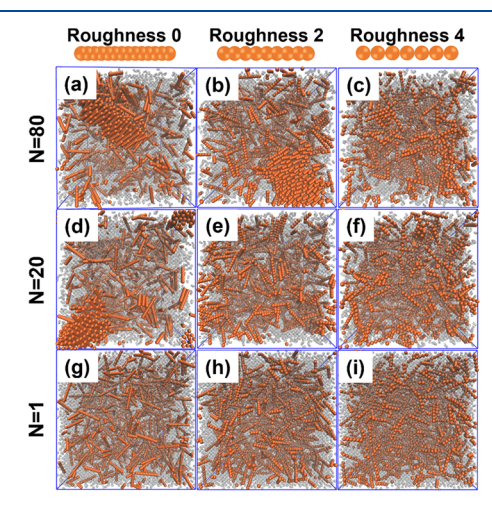


Figure 2. Representative simulation snapshots of PNCs obtained using visual molecular dynamics (VMD)^{S4} with L=7d nanorods of roughness 0, 2, and 4 in the N=80, 20, and 1 matrix at ϕ of 0.16. Matrix beads are depicted as transparent gray beads to view more clearly the (orange/brown) nanorod morphology.

increasing contact peak value of the rod bead—rod bead radial distribution function g(r) (Figure 3a) and increasing orientational order parameter $S_2(r)$ (Figure 3c) of nanorods in the N=80 polymer matrix with decreasing nanorod roughness show a higher propensity of nanorod aggregation and alignment for smoother nanorods. In Figure 3b, the matrix bead—rod bead g(r) for roughness 0 and 2 exhibits a correlation hole region which confirms polymer-depletion-induced nanorod aggregation; in contrast, the lack of a correlation hole in the matrix

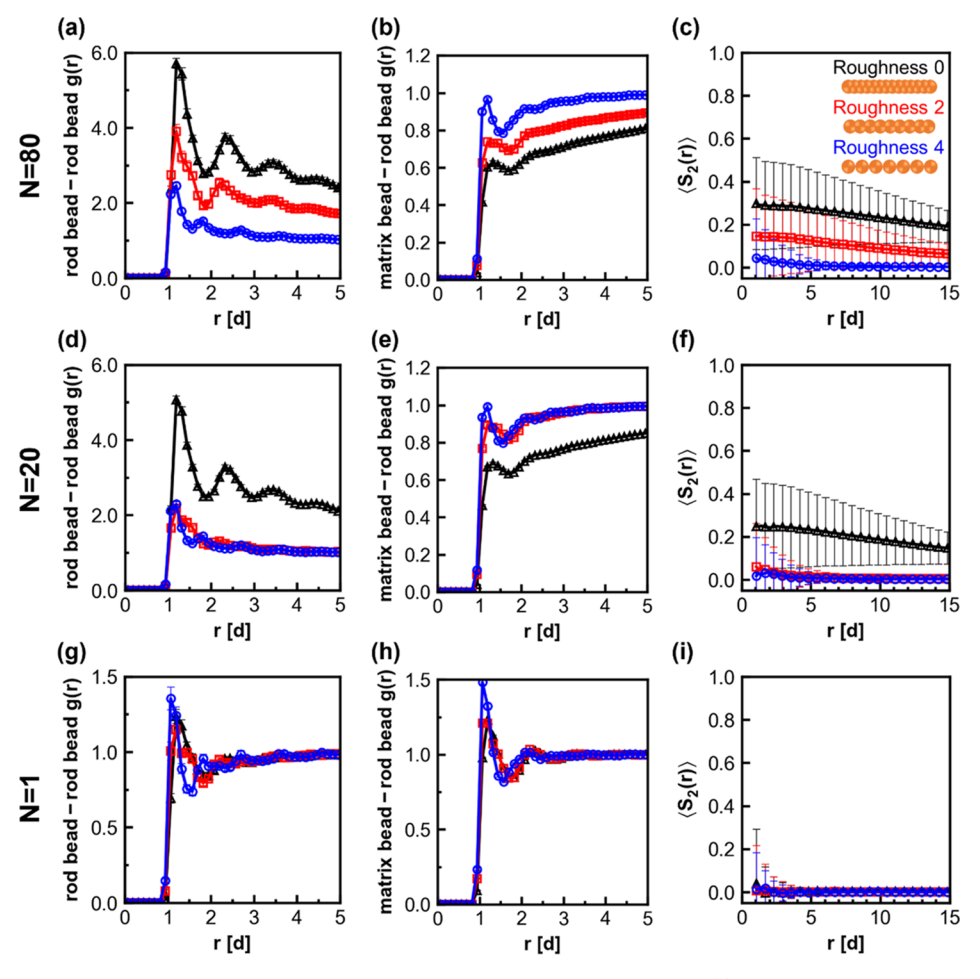


Figure 3. Rod bead—rod bead and matrix bead—rod bead pairwise radial distribution function g(r) and orientational order parameter $\langle S_2(r) \rangle$ for nanorods of roughness 0, 2, and 4 in the N=80, 20, and 1 matrix at ϕ of 0.16. Legend shown in part (c) holds for all plots. Error bars represent the standard deviation from 60 independent configurations, and when not visible, error bars are smaller than the symbol size. Both the rod bead—rod bead g(r) and matrix bead—rod bead g(r) approach 1 at large distances for all three nanorod roughnesses; we only show g(r) at small radial distances to focus on the local packing of nanorods and the matrix polymer.

bead—rod bead g(r) for roughness 4 confirms nanorod dispersion within the polymer matrix. These trends are similar for the N=20 polymer matrix with the only difference being that nanorods with roughness 2 are dispersed in the N=20 matrix. For both the N=80 and N=20 polymer matrices, the chain conformations are not affected by nanorod roughness (Figure S5). In contrast to N=80 and N=20 polymer matrices, in a monomeric (N=1) solvent where each CG solvent bead of diameter 1d represents a collection of small-molecule solvents or an oligomer the same size as the polymer Kuhn segment, the nanorods remain dispersed for all roughness values (Figure 2g-i and Figure 3g-i). Thus, the effect of roughness on nanorods' dispersion or aggregation is dependent on the medium (i.e., N=1 or $N\gg 1$) the nanorods are placed in.

The increased nanorod aggregation and alignment observed for smoother nanorods in a polymer matrix are explained as follows. In PNCs with nanorods being the minority component, the configurational entropy of the polymer chains is a dominant driving force for nanorods to aggregate into bundled structures (similar to that seen experimentally with viruses in polymer solution⁵⁵), much like the depletion attraction between colloids.⁵⁶ The nanorod roughness affects this entropic driving force for depletion—attraction interaction.

This is because at the same D and L the nanorod's occupied volume decreases with increasing roughness, as shown in Figures S1 and S2. Thus, the available volume of the polymer matrix chains which is the difference between the total simulation box volume and the total nanorods' inaccessible volume controls the polymer chain configurational entropy which the system wants to maximize; as the nanorod roughness decreases, the available volume of the polymer matrix decreases, and the system needs to have nanorods aggregated to maximize the volume available to the polymer chains to sample different configurations. Further, this higher entropic driving force for nanorod aggregation for the smoother nanorods is able to overcome the larger effective inter-nanorod repulsion seen in the potential of mean force between two smooth nanorods (roughness = 0) than between two rough nanorods (roughness = 4) (Figure S6). Additionally, the surface of rough nanorods enforces positional order along the axial direction when rough nanorods align in parallel. Going from an unaligned to an aligned state, the loss in configurational entropy of rough nanorods is more than smooth nanorods. Together, these entropic driving forces lead to higher propensity for PNCs with smooth nanorods to exhibit aligned nanorod aggregates than PNCs with rough nanorods.

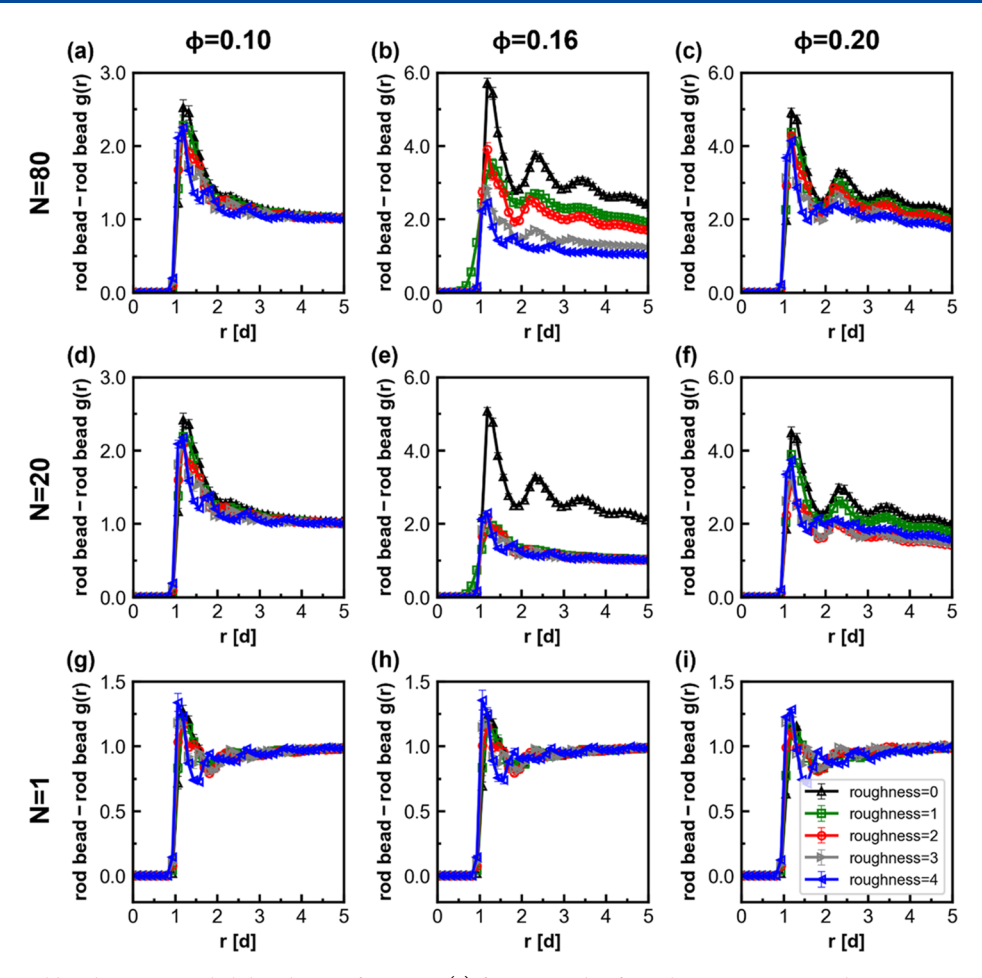


Figure 4. Rod bead—rod bead pairwise radial distribution function g(r) for nanorods of roughness 0, 1, 2, 3, and 4 in N=80, 20, and 1 matrix at ϕ of 0.10, 0.16, and 0.20. The legend shown in part (i) applies for all plots. Error bars represent a standard deviation from 60 independent configurations collected from three simulation trials, and when not visible, error bars are smaller than the symbol size. The rod bead—rod bead g(r) approaches 1 at large distances for all nanorod roughnesses; we only show g(r) at small radial distances to focus on the local packing of nanorods.

In contrast to N=20 and N=80, nanorods remain dispersed for all roughnesses in N=1 further confirming that the conformational entropy of the polymer matrix is a dominant term in the entropic driving forces that is absent in the N=1 system. As a result, at $\phi=0.16$, the depletion—attraction resulting from N=1 is not strong enough to drive L=7d nanorods to aggregate or align regardless of roughness.

In Figures S7 and S8, we present the representative snapshots of the systems at ϕ = 0.10 and 0.20. At ϕ = 0.10, for N = 80, 20, and 1 and at all roughness values, we see the dispersed state of nanorods. At $\phi = 0.20$, the nanorods form aggregates in N = 80 and 20 and remain dispersed in the N = 1matrix; the dispersed state is like the observations for $\phi = 0.16$ (Figure 2) but in the aggregated states, the extent of aggregation is greater at $\phi = 0.20$ than at $\phi = 0.16$. The rod bead—rod bead g(r) in Figure 4 at varying ϕ in N=80 and 20 shows quantitatively that the trend of increasing nanorod roughness leading to decreasing nanorod aggregation in a polymer matrix seen at $\phi = 0.16$ is also seen at $\phi = 0.20$ but to a much smaller extent. At ϕ = 0.10, in N = 80 and 20, the nanorod roughness effects on rod bead-rod bead g(r) are minimal. This nonmonotonic effect of ϕ on the rod bead–rod bead pair correlation is not surprising. At $\phi = 0.20$, nanorods experience strong depletion attraction as compared to $\phi = 0.16$ because of less available volume for the polymer chains at this higher ϕ such that even the roughest nanorods are aggregated,

diminishing the effect of nanorod roughness. In contrast, at ϕ = 0.10, the nanorods' total inaccessible volume is small for all roughness values, diminishing the entropic driving force for nanorod aggregation for all roughness values. In N=1, the nanorod roughness does not affect the rod bead—rod bead g(r) at all three ϕ 's because, as described before, the monomeric solvent does not have the polymer chain conformational entropy term.

The nonmonotonic effect of ϕ on nanorod morphology in the N=80 and N=20 polymer matrices and lack thereof in the N=1 solvent are also reflected in the matrix bead—rod bead g(r) and orientational order parameter $\langle S_2(r) \rangle$ shown in Figures S9 and S10. We also present in Figure S11 the matrix bead—rod bead g(r) plotted up to larger radial distances to show that all the matrix bead—rod bead g(r) values return to a bulk-like correlation of 1 at large distances. We have also calculated the nanorod center-of-mass (COM) radial distribution function presented in Figure S12. The conclusions based on the rod bead—rod bead g(r) remain the same for the nanorod COM—COM g(r).

The results presented so far describing the effect of varying nanorod roughness on positional and orientational order with increasing ϕ lead us to hypothesize that for each nanorod roughness the PNC undergoes a dispersed to aggregated phase transition with increasing ϕ and that this dispersion—aggregation transition volume fraction, $\phi_{\rm D\to A}$, increases with

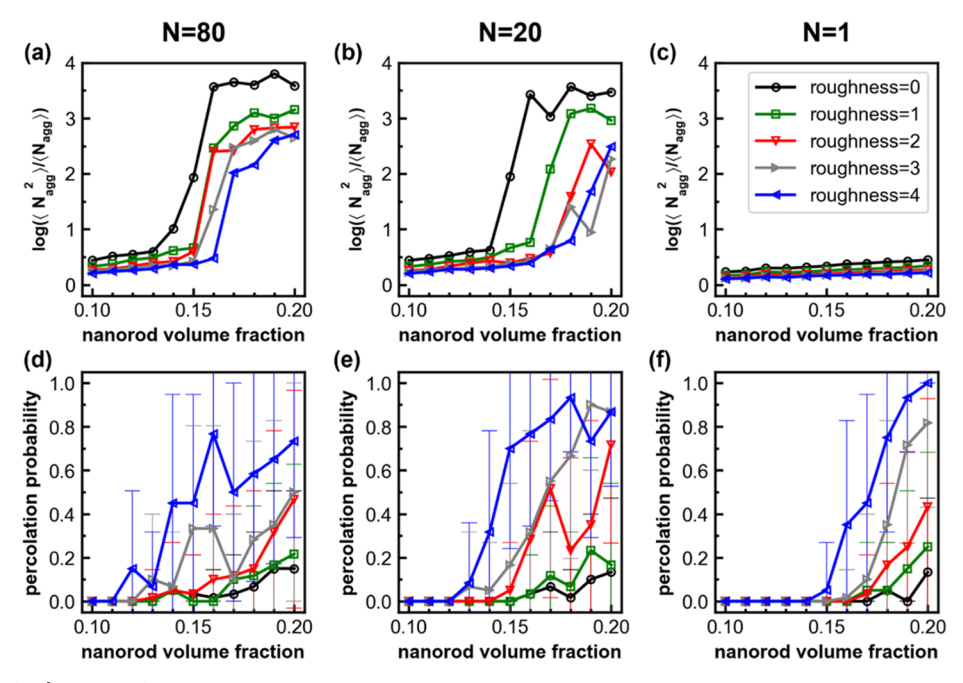


Figure 5. Plots of $\log(\langle N_{\rm agg}^2 \rangle / \langle N_{\rm agg} \rangle)$ and percolation probability for PNCs with L=7d nanorods in matrices of N=80, 20, and 1 as a function of nanorod roughness and nanorod volume fraction, ϕ . In plots of $\log(\langle N_{\rm agg}^2 \rangle / \langle N_{\rm agg} \rangle)$ and percolation probability, the legend shown in part (c) holds for all plots. For $\log(\langle N_{\rm agg}^2 \rangle / \langle N_{\rm agg} \rangle)$ plots, the $\langle \cdots \rangle$ denotes the ensemble averages of 60 independent configurations. For percolation probability plots, the error bars represent standard deviation from 60 independent configurations.

nanorod roughness. To mark the $\phi_{\rm D\to A}$, we quantify the extent of nanorod aggregation by calculating the weight-averaged aggregation number $\langle N_{\rm agg}^2 \rangle / \langle N_{\rm agg} \rangle$. In Figure 5a–5c, the plots of $\log(\langle N_{\rm agg}^2 \rangle / \langle N_{\rm agg} \rangle)$ as a function of ϕ ranging from 0.10 to 0.20 show the dispersion to aggregation transition as a function of ϕ for all roughnesses. We mark $\phi_{\rm D\to A}$ by the value of ϕ at which the $\log(\langle N_{\rm agg}^2 \rangle / \langle N_{\rm agg} \rangle)$ increases sharply (e.g., for N=80 and roughness 4, the $\phi_{\rm D\to A}=0.17$). We find that the $\phi_{\rm D\to A}$ increases with nanorod roughness for both N=80 and 20 matrices, in agreement with our hypothesis. Further, for all roughness values, as N decreases, the $\phi_{\rm D\to A}$ shifts to slightly higher ϕ . In the N=1 matrix, which lacks the polymer chain conformational entropy, there is no such sharp increase, and the values of $\log(\langle N_{\rm agg}^2 \rangle / \langle N_{\rm agg} \rangle)$ are much smaller compared to the analogous case in the polymer matrix because the nanorods remain dispersed.

To quantify percolation, we calculate the percolation probability of the nanorods in these systems (Figures 5d-5f). For PNCs with N=80 (Figure 5d) and N=20(Figure 5e), at every ϕ , percolation probability increases with increasing nanorod roughness. We also note that at higher roughness values of 3 or 4 in the N = 80 matrix and roughness values of 2, 3, and 4 in the N=20 matrix the percolation probability decreases sharply at $\phi_{D\to A}$; we conjecture that the formation of polymer depletion-induced aggregation clusters breaks up the percolation network. The percolation probability of PNCs with smoother nanorods (roughness = 0 and 1) is small and less affected by nanorod aggregation. For the N = 1matrix, we observe percolation for the rougher nanorods (roughness = 3 and 4) at high nanorod volume fraction, ϕ (Figure 5f), without any nanorod aggregation/clustering (Figure 5c).

For all values of N, at the higher values of ϕ , the difference in percolation probability between the smoothest nanorod (roughness = 0) which approaches the spherocylinder nanorod

model and the roughest nanorod (roughness = 4) of connected spheres is significant. One reason for this could be the difference in the occupied volume per nanorod with changing roughness (Figure S1) which, at a fixed ϕ , leads to a higher number density of rough nanorods than smooth nanorods, in turn leading to higher percolation probability. Another reason for the increase in percolation probability with increasing roughness could be the increase in the surface area to volume ratio with increasing roughness. We confirm that the high value of percolation probability observed at high nanorod roughness and at high ϕ is not affected by the chosen simulation box size (see Figure S13 and Table S3). We also show in Figures S14 and S15 that the choice of cutoff distance used in the percolation analysis is appropriate.

In summary, in this letter we have demonstrated using molecular dynamics simulations the effect of nanorod roughness on nanorod aggregation, dispersion, and percolation in polymer nanocomposites (PNCs). By choosing coarsegrained models that enable systematic variation of the nanorod roughness and by selecting purely repulsive pairwise interactions for nanorods and polymer chains, we show how nanorod roughness affects the entropic driving forces for various PNC morphologies. At this entropically driven limit, we find that increasing nanorod roughness hinders nanorod aggregation and promotes nanorod percolation in the polymer melt. As nanorod roughness increases, the nanorod volume fraction needed to induce nanorod aggregation also increases. This increasing nanorod aggregation for decreasing nanorod roughness is explained based on the system wanting to increase the conformational entropy of the polymer chains via depletion-induced attraction between nanorods. To further support this argument about the importance of conformational entropy of the polymer on the observed nanorod roughness effects, we show that by modeling the entire polymer chain as a single coarse-grained matrix bead and mimicking increasing

values of *N* purely with increasing size of that single CG matrix bead we do not observe nanorod aggregation for PNCs with increasing polymer matrix size (Figure S16).

The key design takeaways from this letter are that one may want to create physical roughness on nanorods/nanowires experimentally if percolation at low ϕ is desired. If a bundled array of nanorods with high orientational order is desired, one may want to smooth out the surface roughness in nanorod synthesis to favor depletion-induced aggregation. Computational researchers who choose the type of nanorod model in their simulation studies will note that the observed nanorod phase behavior is clearly dependent on the nanorod model representation: rough "connected bead" nanorod model vs smooth "approaching that of a spherocylinder" model.

ASSOCIATED CONTENT

Supporting Information

The Supporting Information is available free of charge at https://pubs.acs.org/doi/10.1021/acsmacrolett.1c00503.

Additional information on the nanorod roughness model, selected simulation box and system sizes, analysis methods, quantification of polymer matrix chain conformations, additional morphology visualization, and additional results showing the minimal effect of simulation box size, chosen masses, and cutoff distances in analysis (PDF)

AUTHOR INFORMATION

Corresponding Author

Arthi Jayaraman — Department of Chemical and Biomolecular Engineering, University of Delaware, Newark, Delaware 19716, United States; Department of Materials Science and Engineering, University of Delaware, Newark, Delaware 19716, United States; orcid.org/0000-0002-5295-4581; Email: arthij@udel.edu

Author

Shizhao Lu — Department of Chemical and Biomolecular Engineering, University of Delaware, Newark, Delaware 19716, United States

Complete contact information is available at: https://pubs.acs.org/10.1021/acsmacrolett.1c00503

Notes

The authors declare no competing financial interest.

ACKNOWLEDGMENTS

The authors acknowledge financial support from the U.S. National Science Foundation, Grant NSF DMREF #1921871. The computational work in this study was supported by the Caviness High-Performance Computing Community Cluster at University of Delaware and Stampede2 Supercomputing Cluster at Texas Advanced Computing Center (TACC) supported by the Extreme Science and Engineering Discovery Environment (XSEDE).

REFERENCES

(1) Kang, D.; Wang, G.; Huang, Y.; Jiang, P.; Huang, X. Decorating TiO2 nanowires with BaTiO3 nanoparticles: a new approach leading to substantially enhanced energy storage capability of high-k polymer nanocomposites. ACS Appl. Mater. Interfaces 2018, 10 (4), 4077–4085.

- (2) Xie, B.; Zhu, Y.; Marwat, M. A.; Zhang, S.; Zhang, L.; Zhang, H. Tailoring the energy storage performance of polymer nanocomposites with aspect ratio optimized 1D nanofillers. *J. Mater. Chem. A* **2018**, 6 (41), 20356–20364.
- (3) Huang, X.; Sun, B.; Zhu, Y.; Li, S.; Jiang, P. High-k polymer nanocomposites with 1D filler for dielectric and energy storage applications. *Prog. Mater. Sci.* **2019**, *100*, 187–225.
- (4) Singh, R.; Bajpai, A.; Shrivastava, A. CdSe nanorod-reinforced poly (thiophene) composites in designing energy storage devices: study of morphology and dielectric behavior. *Polym. Bull.* **2021**, 78 (1), 115–131.
- (5) Sun, Y. L.; Tang, H. Y.; Ribbe, A.; Duzhko, V.; Woodard, T. L.; Ward, J. E.; Bai, Y.; Nevin, K. P.; Nonnenmann, S. S.; Russell, T.; Emrick, T.; Lovley, D. R. Conductive Composite Materials Fabricated from Microbially Produced Protein Nanowires. *Small* **2018**, *14* (44), 1–5
- (6) Lim, C.; Shin, Y.; Jung, J.; Kim, J. H.; Lee, S.; Kim, D.-H. Stretchable conductive nanocomposite based on alginate hydrogel and silver nanowires for wearable electronics. *APL Mater.* **2019**, *7* (3), 031502.
- (7) Smith, A. F.; Liu, X.; Woodard, T. L.; Fu, T.; Emrick, T.; Jiménez, J. M.; Lovley, D. R.; Yao, J. Bioelectronic protein nanowire sensors for ammonia detection. *Nano Res.* **2020**, *13*, 1479–1484.
- (8) Lovley, D. R.; Yao, J. Intrinsically conductive microbial nanowires for 'green'electronics with novel functions. *Trends Biotechnol.* **2021**, 39, 940.
- (9) Pastoriza-Santos, I.; Kinnear, C.; Pérez-Juste, J.; Mulvaney, P.; Liz-Marzán, L. M. Plasmonic polymer nanocomposites. *Nature Reviews Materials* **2018**, *3* (10), 375–391.
- (10) Wei, W.; Bai, F.; Fan, H. Oriented Gold Nanorod Arrays: Self-Assembly and Optoelectronic Applications. *Angew. Chem., Int. Ed.* **2019**, *58* (35), 11956–11966.
- (11) Hore, M. J. A.; Composto, R. J. Functional polymer nanocomposites enhanced by nanorods. *Macromolecules* **2014**, 47 (3), 875–887.
- (12) Wang, R.; Chen, C.; Zheng, Y.; Wang, H.; Liu, J.-W.; Yu, S.-H. Structure—property relationship of assembled nanowire materials. *Materials Chemistry Frontiers* **2020**, *4* (10), 2881–2903.
- (13) Lu, S.; Wu, Z.; Jayaraman, A. Molecular Modeling and Simulation of Polymer Nanocomposites with Nanorod Fillers. *J. Phys. Chem. B* **2021**, *125* (9), 2435–2449.
- (14) Onsager, L. The effects of shape on the interaction of colloidal particles. *Ann. N. Y. Acad. Sci.* **1949**, *51* (4), 627–659.
- (15) Balberg, I.; Anderson, C.; Alexander, S.; Wagner, N. Excluded volume and its relation to the onset of percolation. *Phys. Rev. B: Condens. Matter Mater. Phys.* **1984**, *30* (7), 3933.
- (16) Schilling, T.; Miller, M. A.; Van Der Schoot, P. Percolation in suspensions of hard nanoparticles: From spheres to needles. *Epl* **2015**, 111 (5), 056004.
- (17) Finner, S. P.; Atashpendar, A.; Schilling, T.; Van Der Schoot, P. Unusual geometric percolation of hard nanorods in the uniaxial nematic liquid crystalline phase. *Phys. Rev. E: Stat. Phys., Plasmas, Fluids, Relat. Interdiscip. Top.* **2019**, *100* (6), 062129.
- (18) Otten, R. H. J.; Van Der Schoot, P. Connectivity percolation of polydisperse anisotropic nanofillers. *J. Chem. Phys.* **2011**, 134 (9), 094902.
- (19) Mutiso, R. M.; Sherrott, M. C.; Li, J.; Winey, K. I. Simulations and generalized model of the effect of filler size dispersity on electrical percolation in rod networks. *Phys. Rev. B: Condens. Matter Mater. Phys.* **2012**, *86* (21), 1–6.
- (20) Nigro, B.; Grimaldi, C.; Ryser, P.; Chatterjee, A. P.; Van Der Schoot, P. Quasiuniversal connectedness percolation of polydisperse rod systems. *Phys. Rev. Lett.* **2013**, *110* (1), 1–5.
- (21) Meyer, H.; Van Der Schoot, P.; Schilling, T. Percolation in suspensions of polydisperse hard rods: Quasi universality and finite-size effects. *J. Chem. Phys.* **2015**, *143* (4), 044901.
- (22) Munson-Mcgee, S. H. Estimation of the critical concentration in an anisotropic percolation network. *Phys. Rev. B: Condens. Matter Mater. Phys.* **1991**, 43 (4), 3331–3336.

- (23) Du, F.; Fischer, J. E.; Winey, K. I. Effect of nanotube alignment on percolation conductivity in carbon nanotube/polymer composites. *Phys. Rev. B: Condens. Matter Mater. Phys.* **2005**, DOI: 10.1103/PhysRevB.72.121404.
- (24) White, S. I.; DiDonna, B. A.; Mu, M.; Lubensky, T. C.; Winey, K. I. Simulations and electrical conductivity of percolated networks of finite rods with various degrees of axial alignment. *Phys. Rev. B: Condens. Matter Mater. Phys.* **2009**, 79 (2), 1–6.
- (25) Finner, S. P.; Schilling, T.; Van Der Schoot, P. Connectivity, Not Density, Dictates Percolation in Nematic Liquid Crystals of Slender Nanoparticles. *Phys. Rev. Lett.* **2019**, *122* (9), 97801–97801.
- (26) Zhao, K.; Mason, T. G. Directing colloidal self-assembly through roughness-controlled depletion attractions. *Phys. Rev. Lett.* **2007**, 99 (26), 268301.
- (27) Zhang, P.; Yang, L.; Li, Q.; Wu, S.; Jia, S.; Li, Z.; Zhang, Z.; Shi, L. Ellipsoidal colloids with a controlled surface roughness via bioinspired surface engineering: building blocks for liquid marbles and superhydrophobic surfaces. ACS Appl. Mater. Interfaces 2017, 9 (8), 7648–7657.
- (28) González-Rubio, G.; Mosquera, J.; Kumar, V.; Pedrazo-Tardajos, A.; Llombart, P.; Solís, D. M.; Lobato, I.; Noya, E. G.; Guerrero-Martínez, A.; Taboada, J. M.; et al. Micelle-directed chiral seeded growth on anisotropic gold nanocrystals. *Science* **2020**, 368 (6498), 1472–1477.
- (29) Banerjee, D.; Yang, J.; Schweizer, K. S. Entropic depletion in colloidal suspensions and polymer liquids: role of nanoparticle surface topography. *Soft Matter* **2015**, *11* (47), 9086–9098.
- (30) Anzini, P.; Parola, A. How roughness affects the depletion mechanism. *Soft Matter* **2017**, *13* (30), 5150–5157.
- (31) Moinuddin, M.; Biswas, P.; Tripathy, M. The effect of surface roughness on the phase behavior of colloidal particles. *J. Chem. Phys.* **2020**, *152* (4), 044902.
- (32) Kamp, M.; Hermes, M.; Van Kats, C. M.; Kraft, D. J.; Kegel, W. K.; Dijkstra, M.; Van Blaaderen, A. Selective depletion interactions in mixtures of rough and smooth silica spheres. *Langmuir* **2016**, *32* (5), 1233–1240.
- (33) Badaire, S.; Cottin-Bizonne, C.; Stroock, A. D. Experimental investigation of selective colloidal interactions controlled by shape, surface roughness, and steric layers. *Langmuir* **2008**, *24* (20), 11451–11463
- (34) Hooper, J. B.; Schweizer, K. S.; Desai, T. G.; Koshy, R.; Keblinski, P. Structure, surface excess and effective interactions in polymer nanocomposite melts and concentrated solutions. *J. Chem. Phys.* **2004**, *121* (14), 6986–6997.
- (35) Toepperwein, G. N.; Karayiannis, N. C.; Riggleman, R. A.; Kröger, M.; De Pablo, J. J. Influence of nanorod inclusions on structure and primitive path network of polymer nanocomposites at equilibrium and under deformation. *Macromolecules* **2011**, *44* (4), 1034–1045.
- (36) Gao, Y.; Liu, J.; Shen, J.; Zhang, L.; Cao, D. Molecular dynamics simulation of dispersion and aggregation kinetics of nanorods in polymer nanocomposites. *Polymer* **2014**, *55* (5), 1273–1281.
- (37) Kim, M. J.; Cho, H. W.; Kim, J.; Kim, H.; Sung, B. J. Translational and rotational diffusion of a single nanorod in unentangled polymer melts. *Phys. Rev. E* **2015**, *92* (4), 042601.
- (38) Shen, J.; Li, X.; Shen, X.; Liu, J. Insight into the Dispersion Mechanism of Polymer-Grafted Nanorods in Polymer Nanocomposites: A Molecular Dynamics Simulation Study. *Macromolecules* **2017**, *50* (2), 687–699.
- (39) Chen, Y.; Xu, Q.; Jin, Y.; Qian, X.; Liu, L.; Liu, J.; Ganesan, V. Design of End-to-End Assembly of Side-Grafted Nanorods in a Homopolymer Matrix. *Macromolecules* **2018**, *51* (11), 4143–4157.
- (40) Erigi, U.; Dhumal, U.; Tripathy, M. Phase behavior of polymer—nanorod composites: A comparative study using PRISM theory and molecular dynamics simulations. *J. Chem. Phys.* **2021**, *154* (12), 124903.

- (41) Toepperwein, G. N.; Riggleman, R. A.; De Pablo, J. J. Dynamics and deformation response of rod-containing nanocomposites. *Macromolecules* **2012**, *45* (1), 543–554.
- (42) Kharazmi, A.; Priezjev, N. V. Molecular dynamics simulations of the rotational and translational diffusion of a Janus rod-shaped nanoparticle. *J. Phys. Chem. B* **2017**, *121* (29), 7133–7139.
- (43) Karatrantos, A.; Composto, R. J.; Winey, K. I.; Clarke, N. Nanorod Diffusion in Polymer Nanocomposites by Molecular Dynamics Simulations. *Macromolecules* **2019**, 52 (6), 2513–2520.
- (44) Wang, J.; O'Connor, T. C.; Grest, G. S.; Zheng, Y.; Rubinstein, M.; Ge, T. Diffusion of Thin Nanorods in Polymer Melts. *Macromolecules* **2021**, *54* (15), 7051–7059.
- (45) Grest, G. S.; Kremer, K. Molecular dynamics simulation for polymers in the presence of a heat bath. *Phys. Rev. A: At., Mol., Opt. Phys.* **1986**, 33 (5), 3628.
- (46) Kamberaj, H.; Low, R.; Neal, M. Time reversible and symplectic integrators for molecular dynamics simulations of rigid molecules. *J. Chem. Phys.* **2005**, 122 (22), 224114.
- (47) Plimpton, S. Fast Parallel Algorithms for Short-Range Molecular Dynamics. *I. Comput. Phys.* **1995**, *117* (1), 1–19.
- (48) Lennard-Jones, J. E. On the Determination of Molecular Fields. II. From the Equation of State of a Gas. *Proc. R. Soc. London A* **1924**, *106* (738), 463–477.
- (49) Weeks, J. D.; Chandler, D.; Andersen, H. C. Role of repulsive forces in determining the equilibrium structure of simple liquids. *J. Chem. Phys.* **1971**, 54 (12), 5237–5247.
- (50) Nosé, S. A unified formulation of the constant temperature molecular dynamics methods. *J. Chem. Phys.* **1984**, *81* (1), 511–519.
- (51) Schweizer, K. S.; Curro, J. G. Integral equation theory of polymer melts: density fluctuations, static structure factor, and comparison with incompressible and continuum limit models. *Macromolecules* **1988**, 21 (10), 3082–3087.
- (52) Honnell, K. G.; Curro, J. G.; Schweizer, K. S. Local structure of semiflexible polymer melts. *Macromolecules* **1990**, 23 (14), 3496–3505.
- (53) Jayaraman, A.; Schweizer, K. S. Structure and assembly of dense solutions and melts of single tethered nanoparticles. *J. Chem. Phys.* **2008**, *128* (16), *164904*.
- (54) Humphrey, W.; Dalke, A.; Schulten, K. VMD: visual molecular dynamics. *J. Mol. Graphics* **1996**, *14* (1), 33–38.
- (55) Yang, Y.; Barry, E.; Dogic, Z.; Hagan, M. F. Self-assembly of 2D membranes from mixtures of hard rods and depleting polymers. *Soft Matter* **2012**, *8* (3), 707–714.
- (56) Asakura, S.; Oosawa, F. On interaction between two bodies immersed in a solution of macromolecules. *J. Chem. Phys.* **1954**, 22 (7), 1255–1256.
- (57) Musino, D.; Genix, A. C.; Chauveau, E.; Bizien, T.; Oberdisse, J. Structural identification of percolation of nanoparticles. *Nanoscale* **2020**, *12* (6), 3907–3915.
- (58) Drwenski, T.; Van Roij, R.; Van Der Schoot, P. Connectedness percolation of hard convex polygonal rods and platelets. *J. Chem. Phys.* **2018**, *149* (5), 054902.